catalysts

MDPI

Article

Comparative Study of Supported Ni and Co Catalysts Prepared Using the All-in-One Method in the Hydrogenation of CO_2: Effects of Using (Poly)Vinyl Alcohol (PVA) as an Additive

Luisa F. Navarrete [1], María Atienza-Martínez [1], Inés Reyero [1], José Carlos Urroz [2], Oihana Amorrortu [3], Oihane Sanz [3], Mario Montes [3], Siby I. Garcés [4], Fernando Bimbela [1] and Luis M. Gandía [1,*]

[1] Institute for Advanced Materials and Mathematics (InaMat2), Departamento de Ciencias, Universidad Pública de Navarra, 31006 Pamplona, Spain; luisa.navarrete@unavarra.es (L.F.N.); maria.atienza@unavarra.es (M.A.-M.); ines.reyero@unavarra.es (I.R.); fernando.bimbela@unavarra.es (F.B.)
[2] Departamento de Ingeniería, Universidad Pública de Navarra, 31006 Pamplona, Spain; josec.urroz@unavarra.es
[3] Departamento de Química Aplicada, Universidad del País Vasco, 20018 San Sebastian, Spain; oihanaamorrortu@gmail.com (O.A.); oihane.sanz@ehu.eus (O.S.); mariomontes1954@gmail.com (M.M.)
[4] Facultad de Ingeniería, Universidad Libre, Bogota 111071, Colombia; siby.garces@unilibre.edu.co
* Correspondence: lgandia@unavarra.es

Abstract: Two series of Ni and Co catalysts supported onto La-Al_2O_3 were prepared and the CO_2 hydrogenation reactions investigated. The catalytic performance was evaluated in terms of the evolution with the reaction temperature of the CO_2 conversion and product (CH_4 and CO) yields, as well as specific activities (TOF) and apparent activation energies. CH_4 was the favored product over both metals while the TOF for CH_4 formation was about three times higher for Ni than Co at 240–265 °C. Metallic particle size effects were found, with the TOF for CH_4 formation decreasing over both Ni and Co as the mean metallic size decreased. In contrast, the TOF for CO formation tended to increase at a decreasing particle size for the catalysts with the smallest Ni particle sizes. The apparent activation energies for Ni and Co were very similar and significantly decreased to values of 73–79 kJ/mol when the metallic dispersion increased. The catalysts were prepared using the all-in-one method, resulting in (poly)vinyl alcohol (PVA) being a key additive that allowed us to enhance the dispersion of Ni and Co to give very effective catalysts. This comparative study joins the few existing ones in the literature in which catalysts based on these metals operated under strictly the same reaction conditions.

Keywords: all-in-one method; Ni catalysts; Co catalysts; CO_2 hydrogenation; Sabatier reaction

Citation: Navarrete, L.F.; Atienza-Martínez, M.; Reyero, I.; Urroz, J.C.; Amorrortu, O.; Sanz, O.; Montes, M.; Garcés, S.I.; Bimbela, F.; Gandía, L.M. Comparative Study of Supported Ni and Co Catalysts Prepared Using the All-in-One Method in the Hydrogenation of CO_2: Effects of Using (Poly)Vinyl Alcohol (PVA) as an Additive. *Catalysts* **2024**, *14*, 47. https://doi.org/10.3390/catal14010047

Academic Editor: Eun Duck Park

Received: 28 December 2023
Revised: 6 January 2024
Accepted: 7 January 2024
Published: 10 January 2024

1. Introduction

Boosted by the flourishment of the Power-to-Gas (PtG) concept [1], Sabatier's reaction has regained great interest—once again, as already occurred in the 1980s [2]—as a means of producing carbon-neutral methane and promoting the integration of renewables into the energy and industry sectors. On this occasion, thanks to the sophisticated computational and experimental tools currently available, this interest goes beyond process development, and a great amount of effort is being devoted to an understanding of the catalytic aspects prevailing at the molecular level in order to establish the criteria for the rational formulation of these catalysts [3,4]. In particular, control over the reaction selectivity is perhaps the principal current goal. This is because the main products—methane and carbon monoxide—are both of great interest, so the selective production of each of them is obviously positive for developing efficient processes aiming at the valorization of CO_2. It is worth noting in this regard how the perspective on CO has changed within the framework of CO_2 hydrogenation research, from being considered an undesired product of the methanation of CO_2 to

a valuable platform chemical, which also boosts research on the reverse water–gas shift reaction (RWGS) [5,6].

The applied and fundamental interest existing around the CO_2 hydrogenation reaction has led to the production of a vast scientific and technical collection of literature that constitutes the experimental and theoretical body of knowledge in this field. All the relevant aspects of the development of a heterogeneous hydrogenation catalyst have been investigated: the nature of the metal; nature, texture and structure of the metal oxide support; metallic particle size effects; metal–support interaction phenomena; behavior of bimetallic formulations and the use of promoters and modifiers [7–9]. The seminal series of papers by Weatherbee and Bartholomew [2,10] provides the first systematic comparative study of the catalytic performance of some of the most active metals (Ni, Fe, Co and Ru) in CO_2 hydrogenation. The support selected was silica, which minimized the influence of the possible effects associated with these catalysts' components. Since then, numerous CO_2 hydrogenation studies have been reported, and several review articles have recurrently addressed this topic over the years [9,11–15]. Emphasis has been put mainly on Ru, which constitutes the state-of-the-art catalysts in terms of its low-temperature activity, selectivity to methane and stability [12,16,17], as well as on Ni [18–20], because this metal presents the best trade-off between availability, costs and catalytic performance. As a result, Ni has been the active phase of choice for most commercial methanation catalysts [7,21].

Cobalt has been recognized for a long time as an active metal for the hydrogenation of CO_2 [7,10]; however, interest in it has concentrated on its activity for CO hydrogenation in syngas to produce long-chain hydrocarbons according to Fischer–Tropsch synthesis (FTS) [22,23]. Nevertheless, in recent years, attention is refocusing on cobalt in an attempt to gain insight into the factors that control the CO_2 hydrogenation selectivity and into the interplay between the several reaction pathways [16,23–39]. In this regard, it is very enlightening to establish parallelisms between the catalytic performances of cobalt and nickel, which is meaningful for the obvious reason of both metals being neighbors in the fourth period of the periodic table of the elements. However, it is surprising that few comparative studies exist on the catalytic performance of Co and Ni with these metals working under exactly the same operating conditions. Since the results from Weatherbee and Bartholomew's research were published [2,10], some works stand out, such as the one by Habazaki et al. [40] on the co-methanation of CO_2 and CO over Ni and Co catalysts prepared from amorphous alloys with Zr. In addition, Mutschler et al. [16] and Villagra-Soza et al. [35] investigated the CO_2 hydrogenation performance of unsupported Fe, Co, Ni and Cu and silica-supported Ni and Co catalysts, respectively. Liang et al. compared alumina-supported Ni and Co catalysts [41], and Liu et al. performed theoretical computational calculations on the CO_2 adsorption and decomposition on Fe, Co, Ni and Cu [42]. Attention has been paid also to bimetallic Ni–Co formulations [35,43–46] with the aim of tuning the catalytic properties of nickel using the formation of alloys with a second metal [47].

The reports by Weatherbee and Bartholomew were the first comparative studies including specific activities for CO_2 hydrogenation [2,10]. Values about six-fold higher for Co/SiO_2 than for Ni/SiO_2 were obtained at 252 °C and 1 atm total pressure. However, the selectivity to CH_4 was significantly higher for the nickel catalyst (77%) than for the cobalt one (42%), which was in turn more selective to CO at comparable CO_2 conversion levels close to 10%. As for the apparent activation energies, very similar values of 79 kJ/mol and 81 kJ/mol were obtained for Co/SiO_2 and Ni/SiO_2, respectively, in the temperature range of 227–257 °C. It was in principle considered that CO_2 methanation proceed via CO hydrogenation, though the rate-determining step could change from C–O bond excision to C species hydrogenation depending on the metal or the reaction conditions, particularly pressure. Liang et al. also found that Co was more active than Ni, in this case in terms of CO_2 conversion and with both metals supported on alumina at contents between 5 and 25 wt. % [41]. No selectivity values were reported though; as judged from the CO_2 conversions and CH_4 and CO yields, the cobalt catalysts were rather more selective to

CH_4. Ni/Al_2O_3 with the lowest metallic content was more selective to CO than CH_4 at temperatures below 500 °C. The results were interpreted with the aid of in situ DRIFTS measurements, and were explained in terms of a cooperative effect between Co and the support affecting the reaction intermediates and facilitating their conversion into CH_4. Mutschler et al. preformed the hydrogenation of CO_2 over unsupported metallic Ni and Co in powder form [16]. The temperature at which the maximum CO_2 conversion was reached was adopted as a measure of the catalytic activity, with the result that cobalt, with 71% conversion at 388 °C, was much more active than nickel (55% at 519 °C). Cobalt was also significantly more selective to CH_4 than nickel, with 99% versus 80% at the maximum CO_2 conversion conditions. As for the apparent activation energies, they were very similar: 77 kJ/mol over Co and 74 kJ/mol over Ni. This fact was interpreted as an indication that the reaction pathways over both metals were also similar, whereas the higher activity of Co was ascribed to a higher availability of the active sites compared to Ni. More recently, Villagra-Soza et al. have investigated the mechanism of CO_2 hydrogenation over monometallic Ni and Co and bimetallic Ni-Co catalysts supported over SiO_2 [35]. In this case, the specific activities for CH_4 formation were found to be higher over Ni than over Co, while the contrary occurred regarding the specific activities for CO formation. Therefore, silica-supported Ni was more selective to CH_4 than the Co counterpart was. These results are in clear contrast with the trends found previously.

This brief overview illustrates that there are still remarkable discrepancies regarding the catalytic performance of two base metals such as Ni and Co in fundamentals aspects of the CO_2 hydrogenation reaction. Within this context, the main objective of the present study is to provide new information on this subject with the aim of contributing to clarifying the reasons for the existing discordance. To this end, Ni and Co catalysts supported on La-modified alumina (La-Al_2O_3) have been investigated under the same reaction conditions. Lanthanides, and especially lanthanum, have been found to behave as promoters of nickel- [48,49] and cobalt-based [50] catalysts in CO_2 hydrogenation. On the other hand, the preparation method employed was the so-called all-in-one method that was originally developed by our groups for the preparation of structured catalysts [51]. It essentially consists of a wet impregnation relying on the preparation of a slurried aqueous suspension containing all the required components (metal precursor, support and additives). This method also allows us to obtain catalysts in powder form with good metallic dispersion [52]. One of the additives employed is (poly)vinyl alcohol (PVA), which helps to improve the rheological properties of the slurry and also reduces the surface tension during the drying step that leads to the catalyst in powder form. In this work, several catalysts were prepared with varying PVA contents in the slurry as well as in the absence of PVA. This has made it possible to verify whether the additive affected the catalytic performance, while, at the same time, a greater number of samples were available to validate the comparative study without having to change key parameters such as, e.g., the metal content.

2. Results and Discussion

2.1. Catalysts Characterization

Table 1 summarizes the main physicochemical properties of the catalysts, which are named in Mx/La-Al_2O_3 notation, with M being Ni or Co and x the PVA content (wt. %) in the all-in-one suspension (see Section 3.1). The results of the elemental analyses indicate that Ni and Co were adequately incorporated into the catalysts since the actual metal contents, ranging between 13.8 wt. % and 15.1 wt. %, are close to the nominal value (15 wt. %). As for the textural properties, the incorporation of the metallic precursors followed by drying and calcination reduced by 12% and 24% the specific surface areas of the Ni0/La-Al_2O_3 and Co0/La-Al_2O_3 catalysts, respectively, when compared with the La-Al_2O_3 support. The pore volume decreased significantly as well. Adding PVA into the suspension had a positive effect in all cases, with the result that the specific surface areas were higher than those of Ni0/La-Al_2O_3 and Co0/La-Al_2O_3, and approached, in

general, the value of the support. There is no a clear trend, however, with respect to the PVA concentration in the suspension.

Table 1. Physicochemical properties of bare La-Al_2O_3 and supported Ni and Co catalysts [a].

Sample	Metal Content (wt. %)	S_{BET} [b] (m^2/g)	V_p [c] (cm^3/g)	d_p [d] (nm)	S_M [e] (m^2/g_{metal})	D [f] (%)	DoR [g] (%)	d_M [h] (nm)
La-Al_2O_3	---	85	0.35	16	--	--	--	--
Ni0/La-Al_2O_3	15.1	73	0.25	13	24	6.3	52	11
Ni0.3/La-Al_2O_3	13.9	82	0.26	13	41	11	57	6.0
Ni0.7/La-Al_2O_3	14.0	89	0.26	12	46	13	58	5.4
Ni1.0/La-Al_2O_3	14.5	82	0.27	12	49	12	56	5.0
Ni1.3/La-Al_2O_3	13.8	97	0.30	12	48	14	52	4.7
Ni1.6/La-Al_2O_3	14.0	84	0.28	12	50	14	54	4.6
Co0/La-Al_2O_3	14.6	64	0.24	14	21	3.1	91	17.4
Co0.2/La-Al_2O_3	14.3	70	0.22	14	41	6.0	51	8.6
Co0.5/La-Al_2O_3	14.3	81	0.24	12	47	7.0	55	8.0
Co1.0/La-Al_2O_3	14.7	92	0.35	14	43	6.4	52	8.1
Co1.6/La-Al_2O_3	14.3	76	0.28	14	42	6.3	52	8.3

[a] Characterization techniques are described in Section 3.2. [b] Specific surface area. [c] Specific pore volume. [d] Average pore diameter. [e] Metallic surface area. [f] Metallic dispersion. [g] Metallic degree of reduction. [h] Average metallic particle size.

The chemisorption measurements revealed that the Ni catalysts prepared using PVA exhibited a higher metallic surface area and dispersion. The average Ni particle size decreased from 11 nm for the catalyst prepared without PVA (Ni0/La-Al_2O_3) to less than 5 nm for the catalysts prepared in the presence of the highest PVA amounts (Ni1.3/La-Al_2O_3 and Ni1.6/La-Al_2O_3), which showed a reasonable Ni dispersion (about 14%) given their relatively high nickel content. These magnitudes showed asymptotical trends with increasing PVA contents in the formulations. Indeed, the changes in the properties were less marked at PVA contents over 1 wt. %. Regarding the Co catalysts, the presence of PVA during the impregnation also had positive effects on the metallic surface areas and metallic dispersions compared to the Co0/La-Al_2O_3 sample. In this case, the formulation with 0.5 wt. % PVA stood out, leading to the highest cobalt dispersion of 7%, while the other PVA contents employed, both lower (0.2 wt. %) and higher (1.0 and 1.6 wt. %), led to similar results. The lowest Co particle size of 8.0 nm resulting from the H_2 chemisorption data and measured for Co0.5/La-Al_2O_3 is about half the one measured for the catalyst prepared in the absence of PVA (17.4 nm for Co0/La-Al_2O_3), which indicates a remarkable effect of the additive on the cobalt dispersion.

The XRD diffraction patterns of the Ni and Co catalysts are shown in Figure 1. The reduction and passivation of the samples allowed us to identify the crystalline phases of nickel and cobalt in a metallic state. All the Ni catalysts present characteristic diffraction peaks that can be ascribed to the spinel nickel aluminate phase ($NiAl_2O_4$), γ-Al_2O_3 and La_2O_3, which decrease in intensity with an increase in the PVA present in the preparation of the catalyst. This suggests that the additive leads to the formation of less ordered oxides in the final catalyst. The peaks related to metallic Ni show a clear reduction in their intensity in the XRD patterns of the catalysts prepared with increasing amounts of PVA in the all-in-one slurry, thus showing a lower crystallite size, in accordance with the higher dispersion of nickel found using CO chemisorption.

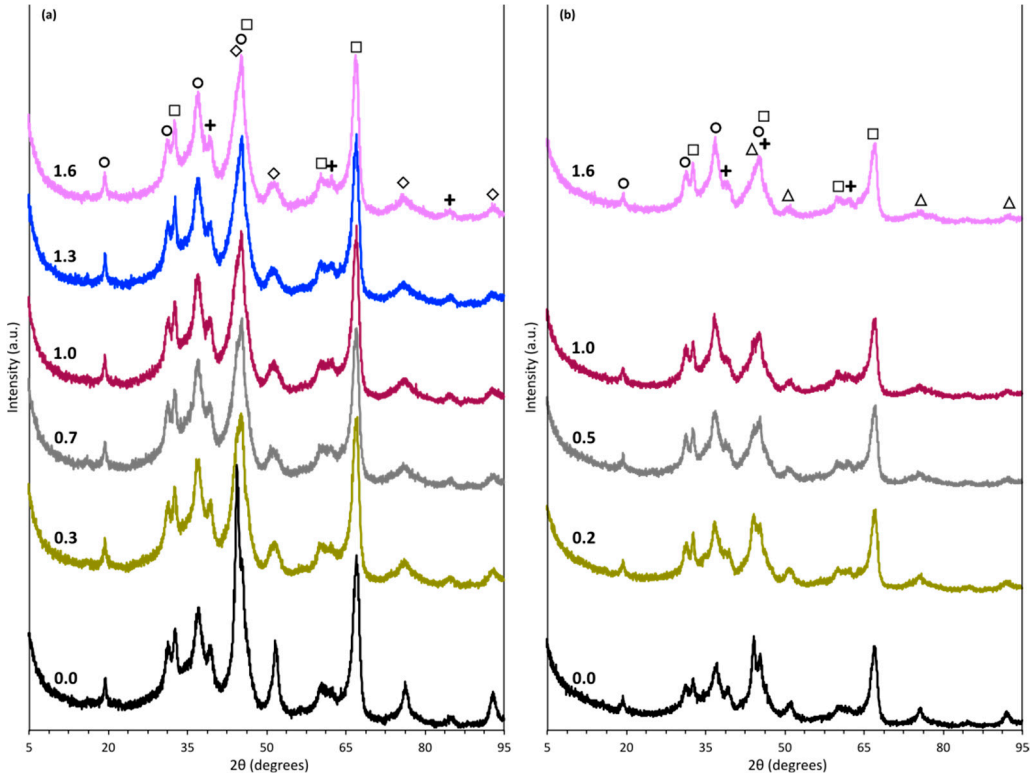

Figure 1. XRD patterns of the reduced and passivated Ni (**a**) and Co (**b**) catalysts prepared with the contents (wt. %) of PVA in the all-in-one suspension indicated in the figures (○: Ni or Co spinel, □: γ-Al_2O_3, +: La_2O_3, ◇: metallic Ni, △: metallic Co).

Regarding the reduced and passivated Co catalysts, apart from metallic cobalt, the XRD patterns revealed characteristic diffraction peaks attributed to the crystalline phases of the La-modified alumina support (γ-Al_2O_3 and La_2O_3), as well as the Co_3O_4 and $CoAl_2O_4$ spinel crystalline phases. These two Co oxide phases present overlapping diffraction peaks, therefore making it impossible to elucidate the actual crystalline structure of the Co/Al catalysts using XRD. However, considering the H_2-TPR profiles, which will be discussed next, it is very likely that both phases coexisted. The formation of crystalline spinel phases is favored by relatively high calcination temperatures during the catalysts' preparation, and surface spinels can already be formed at temperatures as low as 400 °C [53]. As for the PVA content of the slurry used for the catalyst preparation, the XRD patterns clearly show a reduction in the intensity and a broadening of the peaks associated with metallic Co that is consistent with an increased metallic dispersion, as also found for the Ni catalysts.

The H_2-TPR profiles of the calcined catalysts are presented in Figure 2. Including PVA in the all-in-one suspension during the catalysts' preparation clearly modified the reduction characteristics. In addition, the effects in this regard appear to be different for the Ni and Co catalysts. The Ni catalyst prepared without PVA (Ni0/La-Al_2O_3) presented two main reduction events. The first took place starting at temperatures around 300 °C and with a maximum near to 430 °C. Overlapping occurs with the second reduction event, which reaches its maximum at ca. 550 °C and ends at 640 °C. This broad profile indicates that the reduction of various Ni oxide species with different degrees of interaction with the support took place. In particular, the well-dispersed nickel oxide species strongly interacted with the alumina, which are typically reduced in the range of temperature of the second event [54,55].

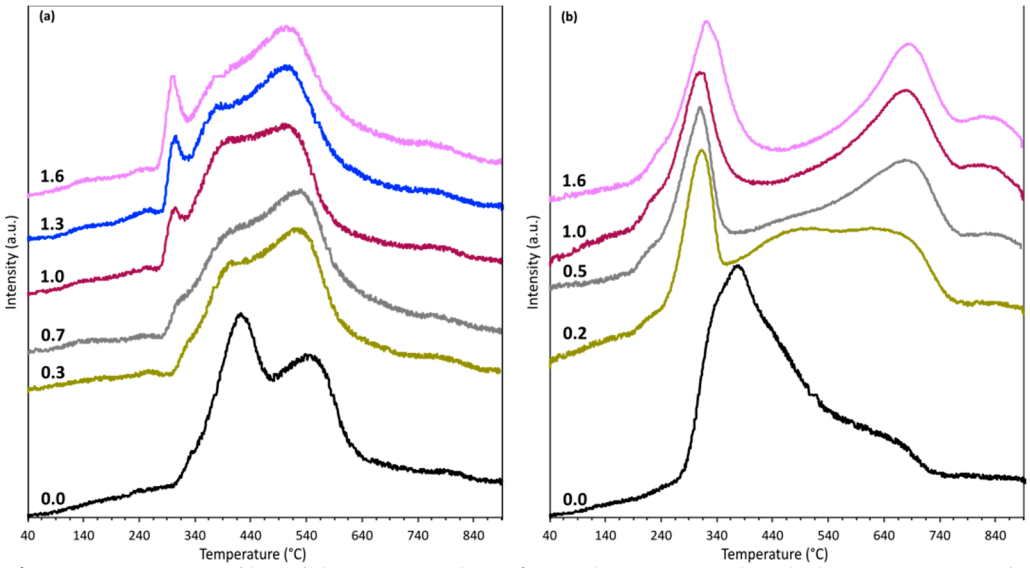

Figure 2. H_2-TPR profiles of the Ni (**a**) and Co (**b**) catalysts prepared with the contents (wt. %) of PVA in the all-in-one suspension indicated in the figures.

When PVA was added to the all-in-one suspension used for the catalysts' preparation, the reduction profile of the resulting samples was dominated by the existence of a very broad reduction region between 300 °C and 640 °C. A small peak appeared at lower temperatures, between 280 °C and 325 °C, when the PVA content was above 0.7 wt. %. The intensity of this low-temperature peak increased concomitantly with the PVA content in the suspension. These results revealed the coexistence of different nickel species with significantly different intensities of interaction with the support. The low-temperature peak is compatible with the presence of bulk NiO weakly interacting with the support. Its appearance at the highest PVA contents in the slurry could be rationalized in terms of the opposite effects being introduced by the additive. On the one hand, at low PVA contents, metallic dispersion is favored, likely due to the additive hindering Ni species coalescence during the catalysts' preparation and/or promoting the metal–support interaction. However, if the PVA content exceeds some given value, hindrance to accommodate all the metal content in a highly dispersed state over the support can occur, causing the formation of bulk NiO. From the chemisorption and the XRD results, it can be inferred that these species were present as relatively small nanoparticles. Three reduction events, including the low-temperature one, have been reported for Ni/La-Al_2O_3 catalysts in previous works [56], likely corresponding to nickel species from weak (bulk NiO) to strong (surface $NiAl_2O_4$) interaction with the support. Finally, the H_2-TPR profiles of the nickel catalysts showed a smooth shift in the reduction events toward lower temperatures as the PVA content of the preparation suspension increased. This fact, together with the development of the low-temperature event, indicate that PVA improves slightly the reducibility of the Ni catalysts.

As for the cobalt catalysts, the reduction of Co/La-Al_2O_3 prepared without PVA (Co0/La-Al_2O_3) started at relatively low temperatures (about 240 °C), showing a large peak centered at 385 °C with a weak but wide shoulder near 630 °C. Such a profile is compatible with the presence in the catalyst precursor of a variety of cobalt oxide species with varied sizes and degrees of interaction with the support [41,57]. The profile shape is also supported by the fact that the Co_3O_4 reduction proceeds in two steps, first into CoO and finally into metallic Co. The predominance of the relatively low-temperature reduction events is compatible with a low dispersion of cobalt, which is in accordance with the mean cobalt particle diameter of 17.4 nm determined for Co0/La-Al_2O_3 (see Table 1). Adding PVA markedly modified the reduction pattern of the Co catalysts. Three peaks with maxima at temperatures around 320 °C, 680 °C and 825 °C were observed in the

H_2-TPR profiles of all the catalysts prepared with PVA added to the all-in-one suspensions. In this case, the increase in the cobalt dispersion from 3% for Co0/La-Al_2O_3 to 6–7% for the samples prepared in the presence of PVA seems to have taken place due to an increased metal–support interaction, with the result being the formation of a significant amount of $CoAl_2O_4$. The partial reduction of cobalt aluminate would lead to a fraction of metallic cobalt particles of a significantly lower mean size (about 8 nm) compared with Co0/La-Al_2O_3. Therefore, PVA seems to improve the cobalt dispersion at the expense of a lower catalyst reducibility, though with a positive final balance since the metallic surface area doubles for the series of Co catalysts prepared in the presence of PVA.

The CO_2-TPD profiles of the calcined catalysts are presented in Figure 3. In order to interpret these results, it should be noted that different ranges of temperature have been defined to distinguish between the types of sites responsible for CO_2 adsorption/desorption [54]. The weakest basic sites are commonly assigned to surface hydroxyls that adsorb CO_2 in the form of bicarbonate that, upon heating, desorb at temperatures below 200–250 °C. It can be seen that those sites are already present in the La-Al_2O_3 support. The incorporation of Ni or Co in the presence of PVA leads to a broadening of the TPD profiles in the low-temperature region, especially in the case of the Ni catalysts, meaning that a greater variety of sites with different strengths are present. The CO_2 desorbed between 200–250 °C and 400–500 °C is assigned to bidentate carbonate species formed over medium-strength basic sites consisting of surface metal–oxide ion pairs. These sites are clearly seen in the CO_2-TPD profile of the support, as well as in the profiles of the cobalt catalysts, although the corresponding desorption peak loses intensity as the PVA content of the all-in-one suspension increases. In the case of the Ni catalysts, rather than an intensity, and therefore, content loss, it seems that these sites lose basic strength as the PVA content increases because the corresponding CO_2-TPD signals shift toward lower temperatures, and end up being part of the low-desorption-temperature weak sites. Finally, the strongest sites correspond to coordinatively unsaturated oxide ions that adsorb CO_2 in the form of monodentate carbonates, which lead to desorption events at the highest temperatures, above 500 °C [20,58]. Strong basic sites are present in the CO_2-TPD profiles of the support and the Ni0 and Co0 catalysts. However, the intensity of the corresponding TPD peak decreases when PVA is used to prepare the catalysts.

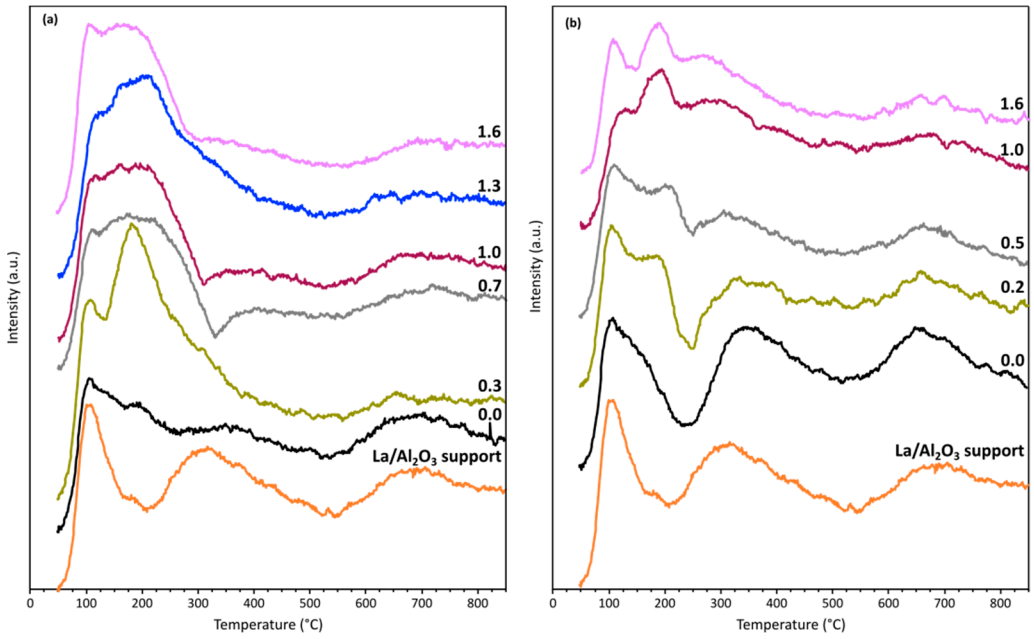

Figure 3. CO_2-TPD profiles of the Ni (**a**) and Co (**b**) catalysts prepared with the contents (wt. %) of PVA in the all-in-one suspension indicated in the figures.

The quantitative results obtained after the integration of the CO_2-TPD peaks are given in Table 2. In accordance with the qualitative description of the TPD profiles, the results confirm the increase in the amount of weak basic sites that takes place following the preparation of the Ni catalysts in the presence of PVA. However, in the case of the Co catalysts, a significant loss of this type of site takes place that varies from 28% for Co0.2/La-Al_2O_3 to 60% for Co1/La-Al_2O_3 and Co1.6/La-Al_2O_3, referred to the support's content. As for the medium-strength and strong basic sites, no distinction has been made in Table 2 due to the lack of sufficient precision to present the results separately. In general, the amount of these types of centers tends to be somewhat higher for the Ni than for the Co catalysts, even though it does not change substantially compared with that of the support. The most salient case is that of Co0/La-Al_2O_3, which exhibits the highest content of medium-strength and strong basic sites. In view of changes in the specific surface area taking place as well, the quantitative results are also given in the form of site density, i.e., per m^2 of catalyst. It can be seen that the conclusions drawn in terms of the amount of CO_2 desorbed per g of catalyst remain valid for the densities of basic sites, so the effects of PVA are not due changes in the specific surface area.

Table 2. Quantitative analysis of the CO_2-TPD results.

Sample	Weak	Medium–Strong	Total [a]	Total [b]
La-Al_2O_3	88	38	126	1.48
Ni0/La-Al_2O_3	43	48	91	1.25
Ni0.3/La-Al_2O_3	201	4	204	2.49
Ni0.7/La-Al_2O_3	114	51	165	1.85
Ni1.0/La-Al_2O_3	113	39	152	1.85
Ni1.3/La-Al_2O_3	176	25	201	2.07
Ni1.6/La-Al_2O_3	109	27	136	1.62
Co0/La-Al_2O_3	50	241	291	4.55
Co0.2/La-Al_2O_3	63	38	101	1.44
Co0.5/La-Al_2O_3	56	35	91	1.12
Co1.0/La-Al_2O_3	35	22	57	0.62
Co1.6/La-Al_2O_3	35	19	54	0.71

[a] CO_2 desorbed in mmol CO_2 per g of catalyst for each category of basic sites. [b] Values expressed in mmol CO_2/m^2.

Thanks to the variation in the amount of PVA used, a series of Ni and another of Co catalysts supported on La-Al_2O_3 have been prepared using the all-in-one method. As a summary of the characterization results, it can be said that the main effect of using the additive has been on the metallic dispersion, increasing it for both Ni and Co, compared with the catalysts prepared without PVA. More profound changes have been introduced into the Co catalysts than into their Ni counterparts. Using PVA promoted the metal–support interaction between Co and La-Al_2O_3, leading to a poorer reducibility. In the case of the Ni catalysts, other effects of PVA, mostly steric, seem to have prevailed. These changes are also reflected in the basic properties since using PVA has been detrimental to both the basicity and basic strength of the cobalt catalysts. In contrast, in the case of the Ni catalysts, using PVA in the all-in-one suspension increased the amount of weak basic sites, thus improving their CO_2 adsorption capacity.

It has been reported that organic additives soluble in water and rich in hydroxyl groups such as polyols have positive effects on the dispersion of Ni in alumina-supported Ni catalysts. The reason would be that the additive prevents the recrystallization of the metallic salt precursor during the drying step. It was proposed that the presence of the additive in the impregnation medium would lead to the formation of an amorphous deposit on the support, whose calcination would finally lead to Ni in a high dispersion state, in contrast with the calcination of the Ni nitrate crystals, which, presumably, finally would produce bigger Ni particles [59]. The adsorption of the organic additive is governed by the formation of hydrogen bonds with protonated surface hydroxyls from the support

surface, with the result being the more homogeneous distribution of the metallic ions due to the steric hindrance introduced for metal species migration [60]. Ribeiro et al. compared Ni catalysts supported on ceria–alumina prepared using conventional incipient wetness impregnation and the all-in-one method employed in the present work [52]. It was found that the all-in-one method improved the nickel dispersion and that, as in our case, the density of the weak basic sites increased as well. These authors argued that surfactants such as PVA affect the metallic particle size due to their capacity to act as capping agents, more specifically due to the formation of a chelating complex with nickel. Similar effects have been described for Co/alumina catalysts prepared using the encapsulation of cobalt nanoparticles in PVA [61]. Positive effects on the catalysts' specific surface area have been reported as well, which is facilitated by the easy removal of PVA upon thermal treatment at relatively mild temperatures of 300–400 °C [62,63]. Finally, Kovalenko et al. have investigated the effects of the concentration and degree of polymerization of PVA [64]. When PVA of a low degree of polymerization was used, it was found that at the lowest additive concentrations, PVA acted as a surfactant. However, on increasing its concentration, its role changed to that of a template, leading to surface deposits of different characteristics in each case. Taking into account that the PVA used in the present work (Mowiol 4-88, Merck, Darmstadt, Germany) is of a low degree of polymerization, the changes in behavior from surfactant to template could relate to the effects introduced by varying the additive content of the all-in-one suspension on the properties of the catalysts considered here.

2.2. Catalytic Performance

Figure 4 shows the time evolution of the CO_2 hydrogenation conversion provided by the nickel (Ni0/La-Al_2O_3 and Ni1/La-Al_2O_3) and cobalt (Co0/La-Al_2O_3 and Co1/La-Al_2O_3) catalysts at a constant reaction temperature of 400 °C and 12 N L $CO_2/(g_{cat}{\cdot}h)$ (GHSV = 5211 h^{-1}). In that figure, the dots represent the average values of the five replicates, and the bars correspond to the 95% confidence interval of these replicates. The stability of the catalytic performance is remarkable; no loss of activity was observed during the experiments. The sum of the CH_4 and CO yields (not shown) was only slightly greater than the corresponding average CO_2 conversion values. The overall mass and atomic C balance closures were very good in all cases (averaging 98 ± 1%). Therefore, the discrepancy between the average CO_2 conversion values and those resulting from the sum of CH_4 and CO yields can be attributed to experimental error. In any case, the differences are less than or equal to 1%. It can be seen that the nickel catalysts were significantly more active than their cobalt counterparts in terms of the CO_2 conversion achieved. In view of the metallic surface areas of the Ni and Co catalysts prepared in the presence of PVA not being very different (see Table 1), this result pointed toward different specific activities for CO_2 hydrogenation over nickel and cobalt.

The evolution of the CO_2 conversion with increasing reaction temperatures in the experiments conducted in dynamic mode (GHSV = 10,422 h^{-1}) with the Ni and Co catalysts with different PVA contents is presented in Figure 5. Moreover, the main results obtained in these tests are summarized in Table 3. T_{50} is the temperature at which the CO_2 conversion reaches 50%, whereas $T^{max}_{XCO_2}$, and $T^{max}_{YCH_4}$ are the temperature values at which the maximum CO_2 conversion and CH_4 yield are attained, respectively.

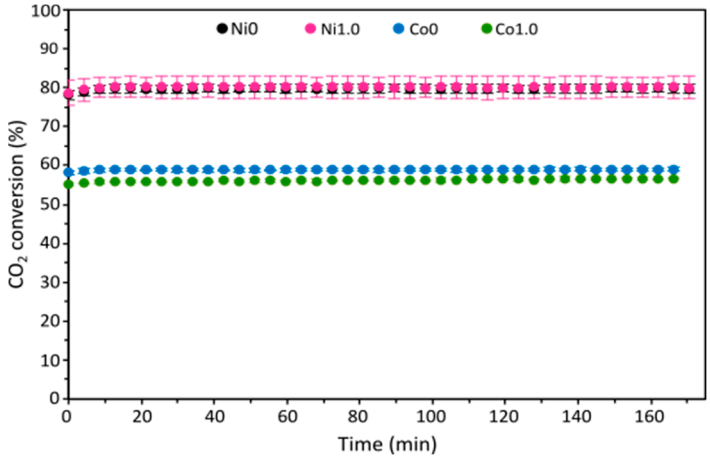

Figure 4. Performance of the Ni0/La-Al_2O_3, Ni1/La-Al_2O_3, Co0/La-Al_2O_3 and Co1/La-Al_2O_3 catalysts during isothermal runs conducted at 400 °C, H_2:CO_2 = 4:1 in the feed stream and 12 N L $CO_2/(g_{cat}{\cdot}h)$ (GHSV = 5211 h^{-1}).

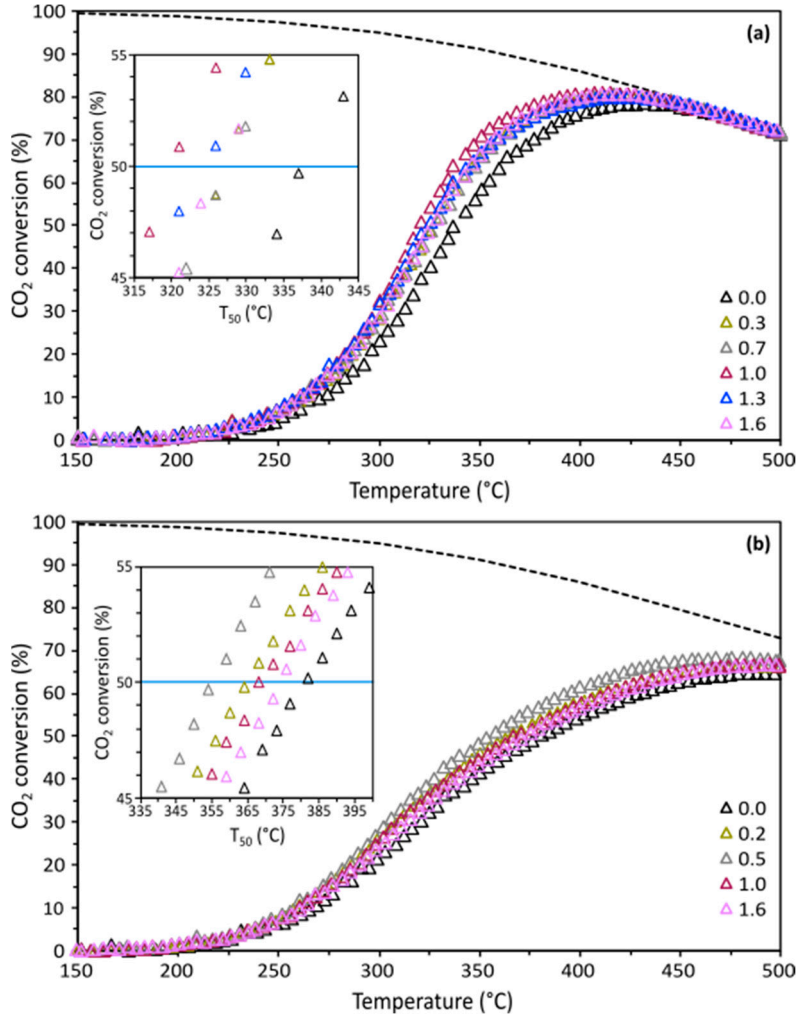

Figure 5. CO_2 conversion at different reaction temperatures in the catalytic tests carried out in dynamic mode: (**a**) Ni catalysts; (**b**) Co catalysts. The insets show the T_{50} values along the blue lines. Reaction conditions: H_2:CO_2 = 4:1 and 24 L N $CO_2/(g_{cat}{\cdot}h)$ (GHSV = 10,422 h^{-1}). Dashed lines correspond to the thermodynamic equilibrium.

Table 3. Summary of the results obtained in the catalytic tests conducted in dynamic mode.

Active Metal	**Ni**						**Co**				
PVA Content (%)	**0.0**	**0.3**	**0.7**	**1.0**	**1.3**	**1.6**	**0.0**	**0.2**	**0.5**	**1.0**	**1.6**
T_{50} (°C)	337	328	327	321	326	327	382	365	355	368	374
$T^{max}_{XCO_2}$ (°C)	432	419	420	411	420	418	501	492	482	488	491
$T^{max}_{YCH_4}$ (°C)	428	419	424	415	412	414	480	471	465	471	478
X_{CO_2max} (%)	78.4	80.2	80.5	80.9	80.0	80.7	64.8	66.1	68.4	66.8	66.5
Y_{CH_4max} (%)	74.6	74.8	76.3	74.2	73.5	74.1	52.9	55.5	58.9	57.5	57.1
Y_{COmax} (%)	6.6	8.5	7.3	9.5	9.5	9.5	13.0	12.9	11.5	10.6	10.8

These results also show that under the same reaction conditions, the nickel catalysts provided higher CO_2 conversions and CH_4 yields than their cobalt counterparts. The nickel catalysts allowed us to reach the equilibrium conversion at about 450 °C. At temperatures above this value, the reaction became thermodynamically controlled over Ni, and no distinction could be made between the catalysts (see Figure 5a). In contrast, the cobalt catalysts did not reach the equilibrium conditions even at 500 °C, which was the highest reaction temperature of the dynamic tests. The difference in T_{50} values was as high as 45 °C between Ni0/La-Al_2O_3 (337 °C) and Co0/La-Al_2O_3 (382 °C). The maximum CH_4 yield attained was much higher over Ni0/La-Al_2O_3 (74.6%) than Co0/La-Al_2O_3 (52.9%) while $T^{max}_{YCH_4}$ was 52 °C lower over Ni0/La-Al_2O_3 (428 °C) than Co0/La-Al_2O_3 (480 °C). As for the effect of the PVA content on the suspensions used for catalyst preparation, it was positive on the CO_2 conversion over both Ni and Co. Taking the corresponding T_{50} values as references, a maximum decrease of 21 °C took place between Ni1/La-Al_2O_3 and Ni0/La-Al_2O_3. This value was close to the difference of 19 °C reached between Co0.5/La-Al_2O_3 and Co0/La-Al_2O_3. However, it is interesting to note how the increase in the conversion has different consequences on the product yields depending on the metal considered. This can be seen in Figure 6, which shows the yields of CH_4 and CO in the dynamic tests performed at increasing reaction temperatures. In the case of Ni, the use of PVA had positive effects on the yields of both CH_4 and CO over the whole temperature range. The yield increase was proportionally higher for CO than CH_4 because the CO yield provided by Ni1/La-Al_2O_3, Ni1.3/La-Al_2O_3 and Ni1.6/La-Al_2O_3 almost doubled that of Ni0/La-Al_2O_3 (see Figure 6c). In contrast, the situation reversed as concerned the cobalt catalysts because the CO yield decreased above 325 °C for the catalysts prepared in the presence of PVA compared to Co0/La-Al_2O_3, whereas it remained almost unaffected at lower temperatures (see Figure 6c). The CH_4 yield, on the other hand, increased for the Co catalysts prepared in the presence of PVA compared to Co0/La-Al_2O_3 over the whole temperature range. In terms of selectivity, it can be said that the selectivity to CO increased over Ni but decreased over Co above 325 °C when the catalysts prepared in the presence of PVA are compared with Ni0/La-Al_2O_3 and Co0/La-Al_2O_3, respectively.

As highlighted in the previous section, the preparation of the catalysts in the presence of PVA improved the dispersion of Ni and Co. Therefore, it is convenient to compare the catalysts' performance in terms of the specific activities. To this end, CO_2 hydrogenation experiments were conducted under a differential conversion regime at temperatures ranging between 230 °C and 275 °C. Figure 7 shows the variation in the TOF values for CH_4 (TOF_{CH4}) and CO (TOF_{CO}) formation with the reaction temperature, mean metallic particle diameter estimated according to chemisorption measurements and PVA content of the suspension employed for the catalysts' preparation.

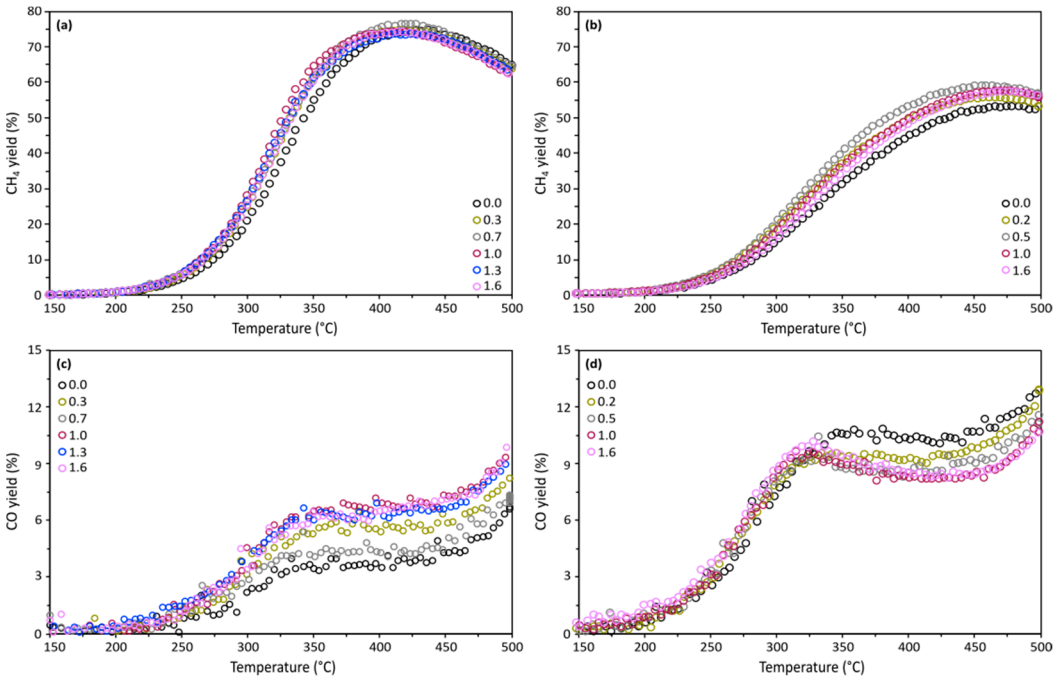

Figure 6. Yields of CH_4 (**a**,**b**) and CO (**c**,**d**) over the Ni (**a**,**c**) and Co (**b**,**d**) catalysts at different reaction temperatures in the catalytic tests carried out in dynamic mode. Reaction conditions: H_2:CO_2 = 4:1 and 24 L N $CO_2/(g_{cat}{\cdot}h)$ (GHSV = 10,422 h^{-1}).

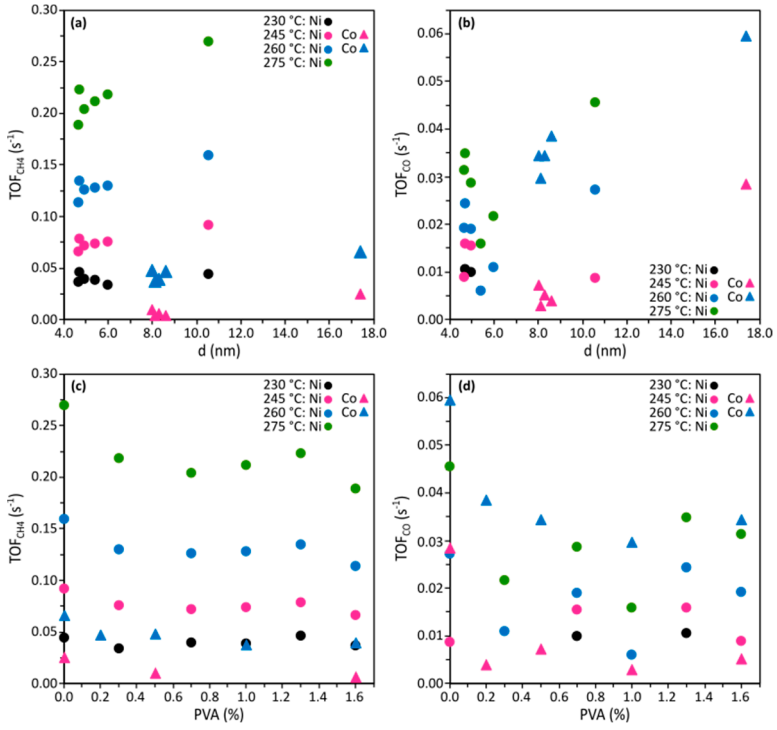

Figure 7. Dependence of the TOF_{CH4} (**a**,**c**) and TOF_{CO} (**b**,**d**) at the reaction temperatures indicated on the mean metallic particle size (**a**,**b**) and the PVA content (**c**,**d**) of the all-in-one suspension used for catalysts' preparation. Circles correspond to the Ni catalysts and triangles to the Co ones.

The comparison between Ni and Co is limited by the fact that no Co catalysts with a mean metallic particle size below 8 nm could be prepared using PVA. In addition, TOF values for cobalt are available only at 245 °C and 260 °C, whereas for nickel, data are

available below 275 °C. Therefore, these restrictions should be taken into account when extrapolating the TOF values (Figure 7) to the product yields (Figure 6). Regardless, it is clear that the specific activity of Ni for CH_4 formation was much higher than that of Co, which is in line with the much higher CH_4 yields provided by the Ni catalysts compared to the Co ones. As for the formation of CO, according to the results obtained at 260 °C (Figure 7b,d), the specific activity was higher for Co than for Ni. However, at 245 °C, the differences between both metals were greatly reduced, and no clear trend could be identified, probably due to the lack of precision associated with the low TOF_{CO} values. As for the metallic particle size effects, TOF_{CH4} decreased for both Ni and Co as the mean metallic particle decreased as well (Figure 7a). The effect of the metallic particle diameter on TOF_{CO} is more difficult to analyze (Figure 7b). For particles above 6 nm, TOF_{CO} decreased as the mean size became smaller for both Ni and Co, whereas below 6 nm, TOF_{CO} increased as the Ni particle size decreased. This increase in the specific activity, together with the increase in the metallic surface area that also took place, could have provoked the increase in the CO yield observed for the Ni catalysts prepared in the presence of PVA (see Figure 6c). Over Co, TOF_{CH4} was only moderately higher than TOF_{CO}, and the specific activities for both products decreased in similar proportions as the Co particle size became smaller. These results are in accordance with the product yield evolution, which showed little effect of the use of PVA on the Co catalyst preparation at low reaction temperatures. While in our work the lowest mean particle size was 8.0 nm for Co0.5/La-Al_2O_3, the same trend of decreasing specific activities can be expected for smaller sizes, following the studies by Iablokov et al. [24].

According to some of the most recent studies, such as the one by Simons et al., CO_2 hydrogenation takes place over nickel according to the RWGS reaction, followed by CO methanation [65]. The authors prepared Ni/SiO_2 catalysts with different metallic contents between 1.7 and 14.6 wt. %, adding citric acid to the impregnation solution, which resulted in a series of catalysts with mean Ni particle sizes between 2 nm and 12 nm. Thanks to operando infrared spectroscopy and isotopic transient experiments, this study claimed that CO_2 dissociates directly over Ni to form strongly chemisorbed surface carbonyls that are subsequently hydrogenated. In addition, the active sites for CO_2 dissociation would be different from those responsible for CO hydrogenation. It was found that TOF_{CH4} decreased and TOF_{CO} increased for catalysts with Ni mean particle sizes below 5 nm, which was attributed to a decrease in the proportion of step edges, which are the active sites for the CO dissociation that takes place as the metallic particle size decreases [65]. These results are very similar to the ones found in the present study, in which TOF_{CH4} decreased and TOF_{CO} increased for the catalysts with Ni particle sizes below 6 nm (see Figure 6a,b).

On the other hand, Villagra-Soza et al. compared silica-supported Ni, Co and bimetallic NiCo catalysts in the hydrogenation of CO_2 under methanation conditions [35]. Isotopic, kinetic and spectroscopic experiments allowed them to conclude that CO_2 hydrogenation followed similar reaction paths over Ni and Co. According to this work, both CH_4 and CO were produced via parallel pathways but with different rate-determining steps. In addition, different types of active sites would be involved in each route. In this regard, CO species strongly adsorbed led to CH_4 formation through the H-assisted dissociation of CO, whereas carbonyls adsorbed weakly would desorb, producing CO. This mechanistic scheme seems compatible with the above-described one by Simons et al. [65]. Particle size effects on the distribution of products during the hydrogenation of CO_2 over cobalt are evidenced at extremely low particle sizes, which were not reached in the present work. Indeed, Zhou et al. prepared silica-supported catalysts with very small Co particle sizes [38]. The catalyst with the smallest nanoparticles (1.6 nm) mainly produced CO through the RWGS reaction, whereas catalysts with nanoparticles not much bigger (2.1–3.0 nm) catalyzed the methanation reaction. It was found that the smallest nanoparticles were fully oxidized in the form of CoO under the reaction conditions, which explained the change in catalytic performance. Recent works have also highlighted the role of oxidized cobalt in the promotion of the RWGS reaction [31,36,66–68].

Finally, another important aspect of the catalytic performance is the apparent activation energy. Thanks to the kinetic experiments, Arrhenius plots could be drawn for the Ni0/La-Al_2O_3, Ni1/La-Al_2O_3, Co0/La-Al_2O_3 and Co1/La-Al_2O_3 catalysts (see Figure 8). Very good fits of the experimental data using linear correlations were obtained in all cases. Both metals provided close apparent energy values for methane formation, which suggests that the reaction pathways over both Ni and Co should be similar. It is interesting to note that that using PVA to prepare the catalysts led to a remarkable decrease in the apparent activation energies from 97–100 kJ/mol for Co0/La-Al_2O_3 and Ni0/La-Al_2O_3 to 73–79 kJ/mol for Co1/La-Al_2O_3 and Ni1/La-Al_2O_3. Villagra-Soza et al. obtained apparent activation energies of 81 kJ/mol and 77 kJ/mol for silica-supported Ni and Co catalysts, respectively, that had the same mean metallic particle diameter of 5 nm [35]. These values are close to the ones found in the present work for Ni1/La-Al_2O_3 and Co1/La-Al_2O_3. It is also worth noting that Wheatherbee and Bartholomew [2,10] obtained 79 kJ/mol for CO_2 hydrogenation over Co/SiO_2 and 81 kJ/mol over Ni/SiO_2 (with a mean Ni particle size of 2.5 nm), which are also similar to the values found here for Ni1/La-Al_2O_3 and Co1/La-Al_2O_3. Taking into account the increase in metallic dispersion provoked by the use of the additive during the catalysts' preparation, the decrease in the activation energy observed could be attributed to particle size effects leading to, e.g., a change in the rate-determining step [10]. In addition, the reduction in the activation energy upon preparing the catalysts in the presence of PVA is another piece of evidence of the positive effects introduced by using the all-in-one preparation method in order to prepare effective Ni and Co catalysts for the CO_2 hydrogenation reaction.

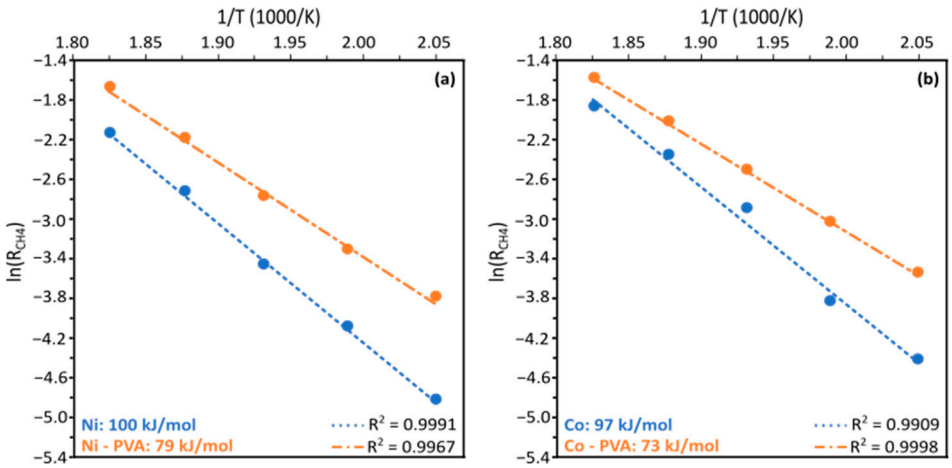

Figure 8. Arrhenius plots for (**a**) Ni0/La-Al_2O_3 and Ni1.0/La-Al_2O_3 and (**b**) Co0/La-Al_2O_3 and Co1.0/La-Al_2O_3 catalysts in CO_2 methanation. Reaction conditions: H_2:CO_2 = 4:1 and 24 L N $CO_2/(g_{cat} \cdot h)$ (GHSV = 10,422 h^{-1}).

Due to structure sensitivity, one has to be very cautious when making comparisons between different results. Meaningful comparisons require analyzing the results obtained using catalysts with close mean metallic particle sizes. In this case, it is particularly important when dealing with very small metallic particles, for which the changes in the proportion of the low coordination number of metallic surface sites such as corners, kinks and edges is more marked, even for slight changes in size. It is remarkable in this regard that some work, such as that by Beierlein et al. [69], concluded that CO_2 hydrogenation over Ni/Al_2O_3 is structure-insensitive. This finding is not necessarily in complete contradiction with other works claiming its highly sensitive character. Beierlein et al. worked with a series of high-loaded Ni catalysts, most of them showing very large Ni particles (5–91 nm). The apparent activation energies changed moderately between 79 kJ/mol and 86 kJ/mol [69]. However, structure sensitivity developed at much lower particle sizes (1–7 nm), as found by Vogt et al. [70].

Whereas proposing a reaction mechanism was not the objective of the present study, the fact that our findings are in accordance with the ones reported by Villagra-Soza et al. [35] and Simons et al. [65] allows us, with the required caution, to assume the reaction schemes proposed in those works. They coincide in attributing a key role to adsorbed car-bonyls as reaction intermediates. The strong adsorption of these species on specific sites such as step edges would lead to CO dissociation and the hydrogenation of the fragments to form CH_4 and H_2O. On the other hand, carbonyls weakly adsorbed would desorb, forming CO as a reaction product. Particle size effects mainly develop for very small metallic particles, which would have a lower proportion of sites capable of adsorbing CO sufficiently strongly compared to larger ones. As the proportion of step edges decreases as the particle size decreases, this would explain the increase in the selectivity to CO that takes place for the very small particles.

3. Materials and Methods

3.1. Catalyst Preparation

Ni/La-Al_2O_3 and Co/La-Al_2O_3 catalysts with nominal metallic contents of 15 wt. % were prepared following the all-in-one method [52] using γ-Al_2O_3 (Sphalerite 505, Axens S.A., Rueil-Malmaison, France) modified with La as the support. First, γ-Al_2O_3 spheres were milled and sieved to collect the particle size distribution comprised within 100 and 200 μm, which was used for the catalyst preparation. After calcination at 500 °C for 2 h, the alumina powder was impregnated to incipient wetness with an aqueous solution of $La(NO_3)_3{\cdot}6H_2O$ (Merck, Darmstadt, Germany) in order to obtain a nominal La content in the final material of 3 wt. %. After the impregnation, the solids were dried at 120 °C for 2 h and calcined at 900 °C for 6 h. The all-in-one method relies on the preparation of a slurried aqueous suspension containing all the required components to obtain the catalyst (metal precursor, support and additives). In this case, Ni or Co nitrates ($Ni(NO_3)_2{\cdot}6H_2O$, $Co(NO_3)_2{\cdot}6H_2O$, Merck, Darmstadt, Germany), a La-modified alumina support, colloidal alumina (Nyacol® Al20, Nanotechnologies Inc., Ashland, MA, USA) as a stabilizing agent, and (poly)vinyl alcohol (PVA, Mowiol 4-88, Merck, Darmstadt, Germany) were employed. The PVA was first dissolved in deionized water at 80 °C in an amount so as to obtain a PVA content of 1 wt. % in the final slurry. After cooling down the solution, Ni or Co nitrate and La-modified alumina were sequentially and slowly added under continuous stirring. Afterward, colloidal alumina was added so as to have a total content of 1 wt. % in the final suspension, which required the addition of water as well (84.6 wt. % of water in the final slurry). The mixture was sonicated for 10 min and then the pH was adjusted to 4 with HNO_3 by adding concentrated acid (65% HNO_3, PanReac, Barcelona, Spain), whereas the pH was monitored. The resulting suspension was kept under stirring for 24 h at room temperature. The catalyst in powder form was finally obtained after drying at 120 °C for 24 h and calcination at 500 °C for 2 h. Catalysts in the absence of PVA were prepared as well. Hereafter, the catalyst samples will be denoted as Mx/La-Al_2O_3, with M being Ni or Co and x corresponding to the PVA content in the final slurried suspension. The values of x were 0.3, 0.7, 1.0, 1.3 and 1.6 wt. % for the Ni catalysts and 0.2, 0.5, 1.0 and 1.6 wt. % for the Co formulation.

3.2. Physicochemical Characterization

Inductively coupled plasma—optical emission spectrometry (ICP-OES) was used to determine the actual Ni and Co contents of the catalysts. The analyses were carried out by the Servicio de Apoyo a la Investigación (SAI) of the Universidad de Zaragoza (Zaragoza, Spain). The N_2 physisorption analyses were measured at 77 K using a Gemini V 2380 (Micromeritics, Norcross, GA, USA) analyzer. Before the measurements, each sample was pre-treated at 200 °C for 2 h under flowing nitrogen. The specific surface area, pore volume and pore size distribution were calculated according to the Brunauer–Emmett–Teller (BET) and Barrett–Joyner–Halenda (BJH) methods, respectively.

The X-ray diffraction (XRD) patterns were recorded using a Bruker D8 ADVANCE (Rheinstetten, Germany) diffractometer with CuKα radiation (λ = 0.154 nm) and a graphite monochromator, operating at 40 kV and 30 mA. The XRD patterns were recorded on the reduced and passivated samples. To this end, the catalysts were reduced in the same conditions before performing the catalytic tests, i.e., under a flow (60 N mL/min) of H_2 at 500 °C for 3 h. Afterward, the sample was cooled down under flowing N_2 until reaching room temperature. Then, passivation was carried out under a flow of 0.5 vol. % O_2 in Ar for 2 h. The samples were scanned within a 2θ range of 5–95° in steps of 0.05° at 5 s per step.

The H_2-TPR experiments were carried out in a AutoChem II 2920 (Micromeritics, Norcross, GA, USA) analyzer. In each of the TPR experiments, 50 mg of the catalyst sample was loaded into a U-shaped quartz reactor and subjected to reduction under 75 N mL/min of a 5% H_2/Ar gas mixture, following a 10 °C/min heating ramp until a final temperature of 900 °C was reached. The hydrogen consumption was recorded using a thermal conductivity detector (TCD). The same apparatus was used to perform the CO_2-TPD measurements as described in a previous work [54].

The metallic surface area and dispersion of the Ni catalysts were obtained from dynamic CO pulse chemisorption measurements at 30 °C using the AutoChem II 2920 (Micromeritics, Norcross, GA, USA) equipment. In the case of the Co catalysts, static volumetric H_2 chemisorption at 35 °C was carried out using a ASAP 2020 (Micromeritics, Norcross, GA, USA) following the double isotherm method. Prior to the analyses, about 50 mg of the samples were reduced in situ under a H_2 gas flow at 500 °C for 3 h. Once the chemisorption experiments were completed, the degree of metal reduction (DOR) was measured by heating the sample up to 430 °C under a He flow of 50 N mL/min and dwelled at the final temperature for 2 h. Then, pulses of a 10% O_2/He mixture were injected until the oxygen consumption ended. The Ni and Co DOR were estimated from the oxygen consumption assuming that the metals were converted into NiO and Co_3O_4, respectively.

3.3. Catalytic Activity

The catalytic tests were carried out under 1.3 atm total pressure, using a Microactivity XS15 system (Micromeritics, Norcross, GA, USA). The gas compositions of the feeding line and of the reaction products were analyzed online using an Agilent 490 (Santa Clara, CA, USA) micro-gas chromatograph equipped with two analysis modules with Molsieve 5Å and PPU chromatographic columns, respectively, each connected to a TCD detector.

The CO_2 hydrogenation tests were carried out in a fixed-bed tubular quartz reactor by loading 50 mg of the catalyst diluted with α-Al_2O_3 (1.10 g; Strem Chemicals, Newburyport, MA, USA) used as an inert filler. The mixed solids were placed inside the reactor between two quartz wool plugs, resulting in a bed volume of 0.64 cm^3. The thermosensitive tip of a K-type thermocouple was exactly placed in contact with the solids at the catalytic bed exit to monitor and control the temperature by means of a proportional integral derivative (PID) controller that regulated the furnace power. Prior to the catalytic tests, the activation of the catalyst was carried out by flowing pure hydrogen (60 N mL/min) at 500 °C for 3 h. A reactor feed stream composed of N_2 (10 vol. %), CO_2 (18 vol. %) and H_2 (72 vol. %) with a H_2:CO_2 molar ratio of 4:1 was used. First, constant-temperature runs were performed with the Ni0/La-Al_2O_3, Co0/La-Al_2O_3, Ni1.0/La-Al_2O_3 and Co1.0/La-Al_2O_3 at 400 °C for 3 h with a spatial velocity of 12 N L CO_2/(g_{cat}·h) (GHSV = 5211 h^{-1}). Five replicates were performed with each catalyst. Next, dynamic activity tests were developed with the Ni0/La-Al_2O_3, Co0/La-Al_2O_3, Ni1.0/La-Al_2O_3 and Co1.0/La-Al_2O_3 in the 215–275 °C temperature range under a spatial velocity of 24 N L CO_2/(g_{cat}·h) (GHSV = 10,422 h^{-1}). The temperature was raised stepwise in increments of 15 °C and the catalytic bed was allowed to operate at each temperature for 120 min. These experiments were performed under a kinetic control regime and at experimental conditions that would allow the performance of differential analysis of the kinetic data. Finally, dynamic tests were also carried out between

150 and 500 °C using all the catalysts prepared in uninterrupted temperature increase mode with a heating rate of 1 °C/min and under a spatial velocity of 24 N L $CO_2/(g_{cat} \cdot h)$.

From the inlet and outlet concentrations of the several compounds and the inlet and outlet total flows, the CO_2 conversion (X_{CO_2}) and yields (Y_i) and selectivities (S_i) to the products (i = CO, CH_4) were calculated according to Equations (1)–(3):

$$X_{CO_2}(\%) = 100 \cdot \frac{F_{CO_{2,in}} - F_{CO_{2,out}}}{F_{CO_{2,in}}} \quad (1)$$

$$Y_i(\%) = 100 \cdot \frac{F_{i,out}}{F_{CO_{2,in}}} \quad (2)$$

$$S_i(\%) = 100 \cdot \frac{Y_i}{X_{CO_2}} \quad (3)$$

where $F_{CO_{2,in}}$ and $F_{CO_{2,out}}$ are the CO_2 molar flow rates at the reactor inlet and outlet, respectively, and $F_{i,out}$ is the outlet molar flow rate of product i.

The turnover frequency (TOF) of the CO_2 hydrogenation process was calculated according to [54]:

$$TOF_{CO_2}\left(s^{-1}\right) = \frac{X_{CO_2} \cdot F_{CO_{2in}} \cdot N_A \cdot A_M}{W_{cat} \cdot S_M} \quad (4)$$

where $F_{CO_{2,in}}$ is given in mol/s; N_A is Avogadro's number (6.02×10^{23} molecules/mol); W_{cat} is the catalyst mass (g_{cat}) in the bed; S_M is the metallic (Ni or Co) surface area in m^2/g_{cat} and A_M the mean area occupied by an exposed Ni or Co atom ($A_{Ni} = 6.77 \times 10^{-20}$ m^2/Ni atom [71], $A_{Co} = 6.85 \times 10^{-20}$ m^2/Co atom [72]).

The TOF values for CH_4 and CO formation can be calculated from Equation (4) as follows:

$$TOF_{CH_4} = TOF_{CO_2} \cdot S_{CH_4} \quad (5)$$

$$TOF_{CO} = TOF_{CO_2} \cdot S_{CO} \quad (6)$$

4. Conclusions

The present comparative study between Ni/La-Al_2O_3 and Co/La-Al_2O_3 catalysts in the hydrogenation of CO_2 has shown that Ni is more active than Co for CH_4 formation, as revealed by taking specific activity measurements. This apparently trivial finding is in contrast with most of the few comparative studies existing in which Ni and Co catalysts have been investigated under rigorously the same reaction conditions. To the best of our knowledge, only a recent work with Ni and Co catalysts supported on silica [35] is completely in line with the results from the present study.

It has been found also that within the range of metallic particle sizes involved in the present study, CH_4 was the product favored over both metals. In addition, the specific activity for CH_4 formation over Ni was about three times higher than over Co at 240–265 °C. The effects of particle size on the specific activities and presumably the apparent activation energies have been found as well. The specific activities for the formation of CH_4 tended to decrease as the metallic particle size decreased for both Ni and Co. In contrast, the specific activity for the formation of CO tended to increase over nickel as the particle diameter decreased for very small particles. In the case of cobalt, no catalysts with sufficiently small metallic particles could be prepared as to identify any clear trend. The apparent activation energies were similar over Ni and Co, suggesting the prevalence of similar reaction paths and rate-determining steps for CO_2 hydrogenation over these metals. The apparent activation energy decreased and remained similar for both Co and Ni in catalysts prepared with relatively small metallic particles.

The catalysts were prepared using the all-in-one method, which relies on the preparation of an aqueous suspension containing all the required components (metal precursor, support and additives). (Poly)vinyl alcohol (PVA) had been revealed as a key additive that allowed us to improve the dispersion of Ni and Co, thus resulting in more effective

hydrogenation catalysts. The positive effects of PVA were limited to low contents in the suspension (below 1 wt. %), at which the additive acted mainly as a surfactant.

Author Contributions: Conceptualization, O.S., M.M., S.I.G., F.B. and L.M.G.; methodology, O.S., M.M., M.A.-M., I.R., F.B. and L.M.G.; formal analysis, L.F.N., O.A., M.A.-M., I.R. and S.I.G.; investigation, L.F.N., O.A., J.C.U., M.A.-M. and I.R.; resources, M.M. and L.M.G.; data curation, L.F.N., O.A., O.S., M.A.-M. and I.R.; writing—original draft preparation, L.F.N., O.A., M.A.-M., I.R., O.S., S.I.G. and F.B.; writing—review and editing, M.M. and L.M.G.; funding acquisition, O.S., M.M., F.B. and L.M.G. All authors have read and agreed to the published version of the manuscript.

Funding: This research was funded by the Spanish Agencia Estatal de Investigación (AEI) and Ministerio de Ciencia e Innovación (MICINN), the European Union's NextGenerationEU funds, the European Regional Development Fund (ERDF/FEDER) "Una manera de hacer Europa" and Plan de Recuperación, Transformación y Resiliencia, grant numbers PID2021-127265OB-C21, TED2021-130846B-I00 and PLEC2022-009221. This research was funded also by the University of the Basque Country, grant numbers COLLAB22/05 and GIU21/033.

Data Availability Statement: Data is contained within the article.

Acknowledgments: The authors would like to acknowledge the use of the Servicio General de Apoyo a la Investigación—SAI, la Universidad de Zaragoza (Zaragoza, Spain). The authors would like to acknowledge Mario Montes on the occasion of his retirement for having been a true catalysis teacher and, even more importantly, a true friend.

Conflicts of Interest: The authors declare no conflicts of interest.

References

1. Bailera, M.; Lisbona, P.; Romeo, L.M.; Espatolero, S. Power to Gas projects review: Lab, pilot and demo plants for storing renewable energy and CO_2. *Renew. Sust. Energy Rev.* **2017**, *69*, 292–312. [CrossRef]
2. Weatherbee, G.D.; Bartholomew, C.H. Hydrogenation of CO_2 on Group VIII Metals: I. Specific Activity of Ni/SiO_2. *J. Catal.* **1981**, *68*, 67–76. [CrossRef]
3. Wang, X.; Shi, H.; Szanyi, J. Controlling selectivities in CO_2 reduction through mechanistic understanding. *Nat. Commun.* **2017**, *8*, 513. [CrossRef] [PubMed]
4. Vogt, C.; Monai, M.; Kramer, G.J.; Weckhuysen, B.M. The renaissance of the Sabatier reaction and its applications on Earth and in space. *Nat. Catal.* **2019**, *2*, 188–197. [CrossRef]
5. González-Castaño, M.; Dorneau, B.; Arellano-García, H. The reverse water gas shift reaction: A process systems engineering perspective. *React. Chem. Eng.* **2021**, *6*, 954–976. [CrossRef]
6. Villora-Picó, J.J.; González-Arias, J.; Pastor-Pérez, L.; Odriozola, J.A.; Reina, T.R. A review on high-pressure heterogeneous catalytic processes for gas-phase CO_2 valorization. *Environ. Res.* **2024**, *240*, 117520. [CrossRef] [PubMed]
7. Mills, G.A.; Steffgen, F.W. Catalytic Methanation. *Catal. Rev.* **1973**, *8*, 159–210. [CrossRef]
8. Wang, Y.; Winter, L.R.; Chen, J.G.; Yan, B. CO_2 hydrogenation over heterogeneous catalysts at atmospheric pressure: From electronic properties to product selectivity. *Green Chem.* **2021**, *23*, 249–267. [CrossRef]
9. Tommasi, M.; Degerli, S.N.; Ramis, G.; Rossetti, I. Advancements in CO_2 Methanation: A Comprehensive Review of Catalysis, Reactor Design and Process Optimization. *Chem. Eng. Res. Des.* **2024**, *201*, 457–482. [CrossRef]
10. Weatherbee, G.D.; Bartholomew, C.H. Hydrogenation of CO_2 on Group VIII Metals. IV. Specific Activities and Selectivities of Silica-Supported Co, Fe and Ru. *J. Catal.* **1984**, *87*, 352–362. [CrossRef]
11. Rönsch, S.; Schneider, J.; Matthischke, S.; Schlüter, M.; Götz, M.; Lefebvre, J.; Prabhakaran, P.; Bajohr, S. Review on methanation—From fundamentals to current projects. *Fuel* **2016**, *166*, 276–296. [CrossRef]
12. Panagiotopoulou, P. Hydrogention of CO_2 over supported noble metal catalysts. *Appl. Catal. A Gen.* **2017**, *542*, 63–70. [CrossRef]
13. Ashok, J.; Pati, S.; Hongmanorom, P.; Tianxi, Z.; Junmei, C. A review of recent catalyst advances in CO_2 methanation processes. *Catal. Today* **2020**, *356*, 471–489. [CrossRef]
14. Lee, W.J.; Li, C.; Prajitno, H.; Yoo, J.; Patel, J.; Yang, Y. Recent trend in thermal catalytic low temperature CO_2 methanation: A critical review. *Catal. Today* **2021**, *368*, 2–19. [CrossRef]
15. Tan, C.H.; Nomanbhay, S.; Shamsuddin, A.H.; Park, Y.-K.; Hernández-Cocoletzi, H.; Show, P.L. Current Developments in Catalytic Methanation of Carbon Dioxide—A Review. *Front. Energy Res.* **2022**, *9*, 795423. [CrossRef]
16. Mutschler, R.; Moioli, E.; Luo, W.; Gallandat, N.; Züttel, A. CO_2 hydrogenation reaction over pristine Fe, Co, Ni, Cu and Al_2O_3 supported Ru: Comparison and determination of the activation energies. *J. Catal.* **2018**, *366*, 139–149. [CrossRef]
17. Gao, X.; Wang, Z.; Huang, Q.; Jiang, M.; Askari, S.; Dewangan, N.; Kawi, S. State-of-art modifications of heterogeneous catalysts for CO_2 methanation—Active sites, surface basicity and oxygen defects. *Catal. Today* **2022**, *402*, 88–103. [CrossRef]

18. Vogt, C.; Monai, M.; Sterk, E.B.; Palle, J.; Melcherts, A.E.M.; Zijlstra, B.; Groeneveld, E.; Berben, P.H.; Boereboom, J.M.; Hensen, E.J.M.; et al. Understanding carbon dioxide activation and carbon–carbon coupling over nickel. *Nat. Commun.* **2019**, *10*, 5330. [CrossRef]
19. Quindimil, A.; De-La-Torre, U.; Pereda-Ayo, B.; Davó-Quiñonero, A.; Bailón-García, E.; Lozano-Castelló, D.; González-Marcos, J.A.; Bueno-López, A.; González-Velasco, J.R. Effect of metal loading on the CO_2 methanation: A comparison between alumina supported Ni and Ru catalysts. *Catal. Today* **2020**, *356*, 419–432. [CrossRef]
20. Shen, L.; Xu, J.; Zhu, M.; Han, Y.-F. Essential Role of the Support for Nickel-Based CO_2 Methanation Catalysts. *ACS Catal.* **2020**, *10*, 14581–14591. [CrossRef]
21. Pearce, B.B.; Twigg, M.V.; Woodward, C. Methanation. In *Catalyst Handbook*, 2nd ed.; Twigg, M.V., Ed.; Manson Publishing: Frome, UK, 1996; pp. 340–383.
22. den Breejen, J.P.; Radstake, P.B.; Bezemer, G.L.; Bitter, J.H.; Frøseth, V.; Holmen, A.; de Jong, K.P. On the Origin of the Cobalt Particle Size Effects in Fischer-Tropsch Catalysis. *J. Am. Chem. Soc.* **2009**, *131*, 7197–7203. [CrossRef] [PubMed]
23. Melaet, G.; Lindeman, A.E.; Somorjai, G.A. Cobalt Particle Size Effects in the Fischer–Tropsch Synthesis and in the Hydrogenation of CO_2 Studied with Nanoparticle Model Catalysts on Silica. *Top. Catal.* **2014**, *57*, 500–507. [CrossRef]
24. Iablokov, V.; Beaumont, S.K.; Alayoglu, S.; Pushkarev, V.V.; Specht, C.; Gao, J.; Alivisatos, A.P.; Kruse, N.; Somorjai, G.A. Size-Controlled Model Co Nanoparticle Catalysts for CO_2 Hydrogenation: Synthesis, Characterization, and Catalytic Reactions. *Nano Lett.* **2012**, *12*, 3091–3096. [CrossRef] [PubMed]
25. Srisawad, N.; Chaitree, W.; Mekasuwandumrong, O.; Shotipruk, A.; Jongsomjit, B.; Panpranot, J. CO_2 hydrogenation over Co/Al_2O_3 catalysts prepared via a solid-state reaction of fine gibbsite and cobalt precursors. *React. Kinet. Mech. Catal.* **2012**, *107*, 179–188. [CrossRef]
26. Zhou, G.; Wu, T.; Xie, H.; Zheng, X. Effects of structure on the carbon dioxide methanation performance of Co-based catalysts. *Int. J. Hydrog. Energy* **2013**, *38*, 10012–10018. [CrossRef]
27. Le, T.A.; Kim, M.S.; Lee, S.H.; Park, E.D. CO and CO_2 Methanation over Supported Cobalt Catalysts. *Top. Catal.* **2017**, *60*, 714–720. [CrossRef]
28. Díez-Ramírez, J.; Sánchez, P.; Kyriakou, V.; Zafeiratos, S.; Marnellos, G.E.; Konsolakis, M.; Dorado, F. Effect of support nature on the cobalt-catalyzed CO_2 hydrogenation. *J. CO2 Util.* **2017**, *21*, 562–571. [CrossRef]
29. Li, W.; Nie, X.; Jiang, X.; Zhang, A.; Ding, F.; Liu, M.; Liu, Z.; Guo, X.; Song, C. ZrO_2 support imparts superior activity and stability of Co catalysts for CO_2 methanation. *Appl. Catal. B Environ.* **2018**, *220*, 397–408. [CrossRef]
30. Jimenez, J.D.; Wen, C.; Lauterbach, J. Design of highly active cobalt catalysts for CO_2 hydrogenation via the tailoring of surface orientation of nanostructures. *Catal. Sci. Technol.* **2019**, *9*, 1970. [CrossRef]
31. Yang, C.; Liu, S.; Wang, Y.; Song, J.; Wang, G.; Wang, S.; Zhao, Z.-J.; Mu, R.; Gong, J. The Interplay between Structure and Product Selectivity of CO_2 Hydrogenation. *Angew. Chem. Int. Ed.* **2019**, *58*, 11242–11247. [CrossRef]
32. Garbarino, G.; Cavattoni, T.; Riani, P.; Busca, G. Support effects in metal catalysis: A study of the behavior of unsupported and silica-supported cobalt catalysts in the hydrogenation of CO_2 at atmospheric pressure. *Catal. Today* **2020**, *345*, 213–219. [CrossRef]
33. Efremova, A.; Rajkumar, T.; Szamosvolgyi, Á.; Sápi, A.; Baán, K.; Szenti, I.; Gómez-Pérez, J.; Varga, G.; Kiss, J.; Halasi, G.; et al. Complexity of a Co_3O_4 System under Ambient-Pressure CO_2 Methanation: Influence of Bulk and Surface Properties on the Catalytic Performance. *J. Phys. Chem. C* **2021**, *125*, 7130–7141. [CrossRef]
34. Tu, J.; Wu, H.; Qian, Q.; Han, S.; Chu, M.; Jia, S.; Feng, R.; Zhai, J.; Hea, M.; Han, B. Low temperature methanation of CO_2 over an amorphous cobalt-based catalyst. *Chem. Sci.* **2021**, *12*, 3937. [CrossRef] [PubMed]
35. Villagra-Soza, F.; Godoy, S.; Karelovic, A.; Jiménez, R. Scrutinizing the mechanism of CO_2 hydrogenation over Ni, Co and bimetallic NiCo surfaces: Isotopic measurements, operando-FTIR experiments and kinetics modelling. *J. Catal.* **2022**, *414*, 1–15. [CrossRef]
36. Wang, M.; Zhang, G.; Zhu, J.; Li, W.; Wang, J.; Bian, K.; Liu, Y.; Ding, F.; Song, C.; Guo, X. Unraveling the tunable selectivity on cobalt oxide and metallic cobalt sites for CO_2 hydrogenation. *Chem. Eng. J.* **2022**, *446*, 137217. [CrossRef]
37. Bredy, P.; Farrusseng, D.; Schuurman, Y.; Meunier, F.C. On the link between CO surface coverage and selectivity to CH_4 during CO_2 hydrogenation over supported cobalt catalysts. *J. Catal.* **2022**, *411*, 93–96. [CrossRef]
38. Zhou, X.; Price, G.A.; Sunley, G.J.; Copéret, C. Small Cobalt Nanoparticles Favor Reverse Water-Gas Shift Reaction Over Methanation under CO_2 Hydrogenation Conditions. *Angew. Chem. Int. Ed.* **2023**, *62*, e202314274. [CrossRef] [PubMed]
39. Yang, F.; Zhang, T.; Zhao, J.; Xiao, J.; Zhou, W. Tuning selectivity of CO_2 hydrogenation over Co catalysts by surface decoration of Sn. *J. Catal.* **2024**, *429*, 115242. [CrossRef]
40. Habazaki, H.; Yamasaki, M.; Zhang, B.-P.; Kawashima, A.; Kohno, S.; Takai, T.; Hashimoto, K. Co-methanation of carbon monoxide and carbon dioxide on supported nickel and cobalt catalysts prepared from amorphous alloys. *Appl. Catal. A Gen.* **1998**, *172*, 131–140. [CrossRef]
41. Liang, C.; Tian, H.; Gao, g.; Zhang, s.; Liu, Q.; Dong, D.; Hu, X. Methanation of CO_2 over alumina supported nickel or cobalt catalysts: Effects of the coordination between metal and support on formation of the reaction intermediates. *Int. J. Hydrog. Energy* **2020**, *45*, 531–543. [CrossRef]
42. Liu, C.; Cundari, T.R.; Wilson, A.K. CO_2 Reduction on Transition Metal (Fe, Co, Ni, and Cu) Surfaces: In Comparison with Homogeneous Catalysis. *J. Phys. Chem. C* **2012**, *116*, 5681–5688. [CrossRef]

43. Xu, L.; Lian, X.; Chen, M.; Cui, Y.; Wang, F.; Li, W.; Huang, B. CO_2 methanation over Co−Ni bimetal-doped ordered mesoporous Al_2O_3 catalysts with enhanced low-temperature activities. *Int. J. Hydrog. Energy* **2018**, *43*, 17172–17184. [CrossRef]
44. Alrafei, B.; Polaert, I.; Ledoux, A.; Azzolina-Jury, F. Remarkably stable and efficient Ni and Ni-Co catalysts for CO_2 methanation. *Catal. Today* **2020**, *346*, 23–33. [CrossRef]
45. Frontera, P.; Malara, A.; Modafferi, V.; Antonucci, V.; Antonucci, P.; Macario, A. Catalytic activity of Ni-Co supported metals in carbon dioxides methanation. *Can. J. Chem. Eng.* **2020**, *98*, 1924–1934. [CrossRef]
46. Shafiee, P.; Alavi, S.M.; Rezaei, M. Solid-state synthesis method for the preparation of cobalt doped Ni–Al_2O_3 mesoporous catalysts for CO_2 methanation. *Int. J. Hydrog. Energy* **2021**, *46*, 3933–3944. [CrossRef]
47. Tsiotsias, A.I.; Charision, N.D.; Yentekakis, I.V.; Goula, M.A. Bimetallic Ni-Based Catalysts for CO_2 Methanation: A Review. *Nanomaterials* **2021**, *11*, 28. [CrossRef] [PubMed]
48. Garbarino, G.; Wang, C.; Cavattoni, T.; Finocchio, E.; Riani, P.; Flytzani-Stephanopoulos, M.; Busca, G. A study of Ni/La-Al_2O_3 catalysts: A competitive system for CO_2 methanation. *Appl. Catal. B Environ.* **2019**, *248*, 286–297. [CrossRef]
49. Ho, P.H.; de Luna, G.S.; Angelucci, S.; Canciani, A.; Jones, W.; Decarolis, D.; Ospitali, F.; Aguado, E.R.; Rodríguez-Castellón, E.; Fornasari, G.; et al. Understanding structure-activity relationships in highly active La promoted Ni catalysts for CO_2 methanation. *Appl. Catal. B Environ.* **2020**, *278*, 119256. [CrossRef]
50. Ferreira, A.C.; Martinho, J.F.; Branco, J.B. Hydrogenation of CO_2 over Cobalt-Lanthanide Bimetallic Oxide Nanofibers. *ChemCatChem* **2022**, *14*, e202101548. [CrossRef]
51. Sousa Aguiar, E.F.; Costa, A.F.; Gandía Pascual, L.M.; Santos, I.B.; Arzamendi Manterola, M.C.; Almeida, L.C.; Montes Ramírez, M.; Odriozola Gordon, J.A. Method for Preparing Structured Catalytic Systems. World Patent WO 2014/085890 AI, 12 June 2014.
52. Ribeiro, A.T.S.; Araújo, I.R.S.; da Silva, E.F.M.; Romano, P.N.; Almeida, J.M.A.R.; Sousa-Aguiar, E.F.; Tomovska, R.; Sanz, O.; Almeida, L.C. Improvement of Ni-based catalyst properties and activity for dry reforming of methane by application of all-in-one preparation method. *J. Mater. Sci.* **2023**, *58*, 3568–3581. [CrossRef]
53. Cesteros, Y.Y.; Salagre, P.; Medina, F.; Sueiras, J.E. Preparation and Characterization of Several High-Area $NiAl_2O_4$ Spinels. Study of Their Reducibility. *Chem. Mater.* **2000**, *12*, 331–335. [CrossRef]
54. González-Rangulan, V.V.; Reyero, I.; Bimbela, F.; Romero-Sarria, F.; Daturi, M.; Gandía, L.M. CO_2 Methanation over Nickel Catalysts: Support Effects Investigated through Specific Activity and Operando IR Spectroscopy Measurements. *Catalysts* **2023**, *13*, 448. [CrossRef]
55. Aljishi, A.; Veilleux, G.; Lalinde, J.A.H.; Kopyscinski, J. The effect of synthesis parameters on ordered mesoporous nickel alumina catalyst for CO_2 methanation. *Appl. Catal. A Gen.* **2018**, *549*, 263–272. [CrossRef]
56. Guilera, J.; Del Valle, J.; Alarcón, A.; Díaz, J.A.; Andreu, T. Metal-oxide promoted Ni/Al_2O_3 as CO_2 methanation micro-size catalysts. *J. CO2 Util.* **2019**, *30*, 11–17. [CrossRef]
57. Gandía, L.M.; Montes, M. Effect of the reduction temperature on the selectivity of the high temperature reaction of acetone and hydrogen over alumina and titania supported nickel and cobalt catalysts. *J. Mol. Catal.* **1994**, *94*, 347–367. [CrossRef]
58. Italiano, C.; Llorca, J.; Pino, L.; Ferraro, M.; Antonucci, V.; Vita, A. CO and CO_2 methanation over Ni catalysts supported on CeO_2, Al_2O_3 and Y_2O_3 oxides. *Appl. Catal. B Environ.* **2020**, *264*, 118494. [CrossRef]
59. Bentaleb, F.; Che, M.; Dubreuil, A.-C.; Thomazeau, C.; Marceau, E. Influence of organic additives on the properties of impregnation solutions and on nickel oxide particle size for Ni/Al_2O_3 catalysts. *Catal. Today* **2014**, *235*, 250–255. [CrossRef]
60. Ryczkowski, J.; Grzegorczyk, W.; Nazimek, D. Support modification with organic reagents and its influence on the development of metal active surface areas in Ni/Al_2O_3 catalysts. *Appl. Catal. A Gen.* **1995**, *126*, 341–349. [CrossRef]
61. Hatamie, S.; Ahadian, M.M.; Rashidi, A.; Karimi, A.; Akhavan, O. Novel synthesis of cobalt/poly vinyl alcohol/gamma alumina nanocomposite for catalytic application. *Appl. Phys. A* **2017**, *123*, 341. [CrossRef]
62. Mateos-Pedrero, C.; Azenha, C.; Pacheco Tanaka, D.A.; Sousa, J.M.; Mendes, A. The influence of the support composition on the physicochemical and catalytic properties of Cu catalysts supported on Zirconia-Alumina for methanol steam reforming. *Appl. Catal. B Environ.* **2020**, *277*, 119243. [CrossRef]
63. Munnik, P.; de Jongh, P.E.; de Jong, K.P. Recent Developments in the Synthesis of Supported Catalysts. *Chem. Rev.* **2015**, *115*, 6687–6718. [CrossRef] [PubMed]
64. Kovalenko, V.; Kotok, V.; Zima, O.; Nafeev, R.; Verbitsky, V.; Melnyk, O. Definition of the Role of Polyvinylalcohol during Formation and in the Structure of Cathodic Synthesized Composite Electrochromic Nickel Hydroxide Layer: Template or Surfactant. *East.-Eur. J. Enterp. Technol.* **2022**, *2*, 6–14. [CrossRef]
65. Simons, J.F.M.; de Heer, T.J.; van de Poll, R.C.J.; Muravev, V.; Kosinov, N.; Hensen, E.J.M. Structure Sensitivity of CO_2 Hydrogenation on Ni Revisited. *J. Am. Chem. Soc.* **2023**, *145*, 20289–20301. [CrossRef] [PubMed]
66. Zhao, K.; Calizzi, M.; Moioli, E.; Li, M.; Borsay, A.; Lombardo, L.; Mutschler, R.; Luo, W.; Züttel, A. Unraveling and optimizing the metal-metal oxide synergistic effect in a highly active $Co_x(CoO)_{1-x}$ catalyst for CO_2 hydrogenation. *J. Energy Chem.* **2021**, *53*, 241250. [CrossRef]
67. Parastaev, A.; Valery Muravev, V.; Huertas Osta, E.; Kimpel, T.F.; Simons, J.F.M.; van Hoof, A.J.F.; Uslamin, E.; Zhang, L.; Struijs, J.J.C.; Burueva, D.B.; et al. Breaking structure sensitivity in CO_2 hydrogenation by tuning metal–oxide interfaces in supported cobalt nanoparticles. *Nat. Catal.* **2022**, *5*, 1051–1060. [CrossRef]
68. ten Have, I.C.; Kromwijk, J.J.G.; Monai, M.; Ferri, D.; Sterk, E.B.; Meirer, F.; Weckhuysen, B.M. Uncovering the reaction mechanism behind CoO as active phase for CO_2 hydrogenation. *Nat. Commun.* **2022**, *13*, 324. [CrossRef] [PubMed]

69. Beierlein, D.; Häussermann, D.; Pfeifer, M.; Schwarz, T.; Stöwe, K.; Traa, Y.; Klemm, E. Is the CO_2 methanation on highly loaded Ni-Al_2O_3 catalysts really structure sensitive? *Appl. Catal. B-Environ.* **2019**, *247*, 200–219. [CrossRef]
70. Vogt, C.; Groeneveld, E.; Kamsma, G.; Nachtegaal, M.; Lu, L.; Kiely, C.J.; Berben, P.H.; Meirer, F.; Weckhuysen, B.M. Unravelling structure sensitivity in CO_2 hydrogenation over nickel. *Nat. Catal.* **2018**, *1*, 127–134. [CrossRef]
71. Bartholomew, C.H.; Pannell, R.B.; Butler, J.L. Support and Crystallite Size Effects in CO Hydrogenation on Nickel. *J. Catal.* **1980**, *65*, 335–347. [CrossRef]
72. Reuel, R.C.; Bartholomew, C.H. The Stoichiometries of H_2 and CO adsorptions on Cobalt: Effects of Support and Preparation. *J. Catal.* **1984**, *85*, 63–77. [CrossRef]